Journal of Visualization, Vol. 9, No. 4 (2006)445-455

Application of Modal Wavelets to PIV Measurements by Selecting Basis Function

Tanaka, K.*[1], Takei, M.*[2], Saito, Y. *[3] and Doh, D. H.*[4]

*1 Okamoto Industries Inc., 3-27-12,Hongo, Bunkyo-ku Tokyo 113-8710, Japan.
E-mail: cpt.tanaka@imx.okamoto-inc.co.jp
*2 Department of Mechanical Engineering, Nihon University, Tokyo, Japan.
*3 Faculty of Engineering, Hosei University, Tokyo, Japan.
*4 Division of Mechanical and Information Engineering, Korea Maritime University, Busan, Korea.

Received 14 April 2006
Revised 4 August 2006

Abstract: A modal wavelet transform, which overcomes the intrinsic data number limitation of power of two to conventional wavelet transform, has been applied to analysis of axial and eddy pseudo velocity fields, standard PIV velocity field and experimental PIV measurement. The modal wavelet transform is compared with the discrete wavelet transform in order to select the optimum basis function among Neumann, Dirichlet and Green function types basis functions. Consequently, it is verified that Neumann type function is the best basis because the correlation of Neumann type basis function is higher and the root mean square is lower than the other basis functions. Also, the decomposition vector patterns by Neumann type are similar to that by conventional Daubechies basis function of 4th order.

Keywords: Modal wavelet transform, Discrete wavelet transform, PIV, Image analysis, Wavelet basis.

1. Introduction

PIV (Particle Image Velocimetry) is utilized widely and generally as an measurement technology for visualizing the velocity distribution of fluid flow (Christensen et al., 2005; Kim et al., 2004). From the obtained velocity distribution by the PIV, the more accurate analysis is also performed by extracting the features of the more detailed flow structure, or removing the noise. The continuous wavelet transform (Farge, 1992) has been utilized as a method of the noise removal and a method of extracting the features of the detailed flow field from a PIV image. For example, Camussi (2002) performed characteristic extraction of eddy structure by using the continuous wavelet transform based on the Mexican hat function for a PIV velocity distribution of a jet. Schram et al. (2004) performed characteristic extraction of eddy structure by using the continuous wavelet transform based on the Maar function for a PIV velocity distribution of back step flow. Özsoy et al. (2005) performed characteristic extraction of eddy structure by using the continuous wavelet transform based on Maar function for a PIV velocity distribution of a cavity flow. However, the velocity field cannot be analyzed in a multiresolution level since this continuous wavelet transform is not an orthonormal. Therefore, recently the discrete wavelet transform that can perform multiresolution analysis at each frequency has been developed (Hernandes et al., 1996). For example, Li et al. (1999) removed the noise and extract the flow structure by using discrete wavelet analysis based on the

Daubechie function for the concentration jet image, whereas Weng et al. (2001) removed the noise by using the discrete wavelet transform that based on the Mallat function for the PIV velocity distribution. Li et al. (2002) performed the characteristic extraction by using the discrete wavelet transform for a PIV velocity distribution of lobbed jet.

As mentioned in the above, wavelet transform is very effective to extract characteristic of detailed flow structure from a PIV velocity distribution. However, there is a disadvantage that it is impossible to use the discrete wavelet transform if the number of the analyzed data is not power of two. In order to solve this disadvantage, Saito (2002) made the basis function by the modal matrix obtained from the governing equation of an image, and proposed a new wavelet transform, called modal wavelet transform. The modal wavelet was applied to the electromagnetic field analysis even if the number of data is not power of two (Endo et al., 2002).

In this study, the effectiveness of the modal wavelet transform in comparison with the discrete wavelet transform is evaluated. A modal wavelet transform and a discrete wavelet transform are conducted to pseudo, standard and experimental vector PIV images of 16 pixel ×16 pixel. It aims to select the most effective basis function of the modal wavelet transform in comparing each basis function from the result of integrated multiresolution.

2. Theory of Modal Wavelet Transform

2.1 Derivation of Basic Equation

The Poisson equation is assumed as the governing equation of image by Saito (2002):

$$\varepsilon \nabla^2 U = -\sigma \,. \tag{1}$$

Where ε is a middle parameter of the image, U is the scalar potential and σ is the source densities of the image of Laplace operator. Because scalar potential U of a pixel in the Eq. (1) is continuous quantity, it can be discretized by the differential calculus system and integral calculus system. As differential calculus system, the finite three points difference method that assumed a pixel position a node is used. When each image pixel is described for the scalar potential U related to the space differential calculus, the Eq. (2) can be obtained:

$$\nabla^2 U = \frac{\partial^2 U_x}{\partial x^2} \cong \frac{U_{x-h} - 2U + U_{x+h}}{h^2} \tag{2}$$

where x is a node ($x = 1, 2, \ldots, n-1, n$) and h is the distance between nodes. When the Eq. (2) is shown in one dimensional matrix of the image data, the Eq. (1) can be written as

$$LU = S \tag{3}$$

When this Eq. (3) is applied to the two dimensional image data, the Eq. (3) can be shown as the Eq. (4):

$$LUL^T = S \tag{4}$$

T indicates the transpose matrix. Because the image U has the $n_x \times n_y$ pixel in the row and column, L is the symmetric matrix of the row n_x and the column n_y with a characteristic of normal value as the Laprashian and the coefficient matrix, S is an image of the source density with the pixel of $n_x \times n_y$. As a boundary condition of coefficient matrix L, the condition is shown in two types which are the Diricret and the Neumann types. On the other hand, because the boundary value problem of liner differential equation is changed to an integral equation by using the Green function, the Eq. (1) can be given as

$$U = \frac{1}{\varepsilon} \int g(r) \sigma dr \tag{5}$$

Because the Green function $g(r)$ in the Eq. (5) becomes infinite when the function is $g(0)$, the minimum distance is assumed to $r_{i,j} = 1$, and the initial condition is assumed to the Eq. (6).

$$g(r) \cong \frac{1}{r_{i,j}} \quad (i \neq j) \quad , \quad g(r) = 1 \quad (i = j) \tag{6}$$

Here, i and j indicate the distance between the source ($i = 1, 2, \ldots, n-1, n$) and the reference ($j =$

1,2,...,n-1,n). When the Eq. (6) is discritized and expressed in matrix, the equation can be shown as

$$\boldsymbol{U} = G\boldsymbol{S} \quad , \; G^{-1}\boldsymbol{U} = \boldsymbol{S} \tag{7}$$

When an image is $n_x \times n_y$ pixel in the row and column, G^{-1} is the symmetric matrix of the row n_x and the column n_y, and the coefficient matrix that has the characteristic of a normal value. In addition, when this Eq. (7) is applied to the two dimensional image data and displayed in the matrix, this equation can be shown in:

$$G^{-1}U(G^{-1})^T = S \tag{8}$$

The discrete wavelet transform that is represented by typical Daubechies basis function has a characteristic shown as

$$W^T W = I \tag{9}$$

where W is the orthonormal basis function. I is the unit matrix having the same order as the basis function W. When the scalar potential U has "a" element, there are "a" orthonormal eigen value λ_i(i= 1, 2, ..., n -1, n) because the coefficient matrix L and G^{-1} are positive definite symmetric matrix, And there are eigen vector v_i(i= 1, 2, ..., n-1, n) corresponding to the eigen value λ_i. Here, this eigen vector is a column vector. The modal matrix W can be shown as

$$W = \begin{bmatrix} v_1 & v_2 & \cdots & v_{a-1} & v_a \end{bmatrix} \quad , \; v_i = \begin{bmatrix} v_{i,1} & v_{i,2} & \cdots & v_{i,a} \end{bmatrix}^T \tag{10}$$

Here, because the modal matrix W in the Eq. (10) is the orthonormal system, it has a characteristic shown in Eq. (9).

The modal matrix W consisting of the eigen vector as the column vector can be used as the basis function of the discrete wavelet transform. The wavelet transform that uses this modal matrix as a basis function is called a modal wavelet transform (Saito, 2002). In the basis function of the modal wavelet transform, there are three types of the Neumann type, the Dirichlet type calculated by the differential calculus system of the Eq. (4), and the Green function type calculated by the integral calculus system of the Eq. (7) . The basis functions to $n_x \times n_y$ = 16 pixel × 16 pixel are shown in Figs. 1(a)-(c). The typical discrete Daubechies basis function of 4th order is shown in Fig. 1(d).

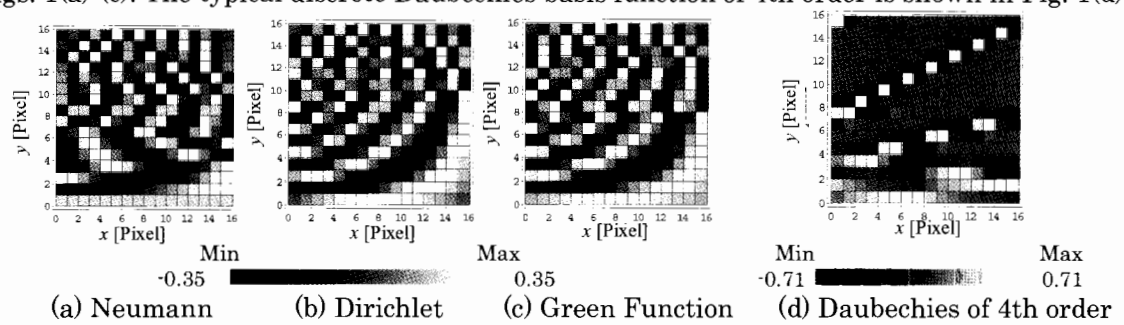

Fig. 1. Basis Functions of modal wavelets.

2.2 Characteristics of Basis Function and Multiresolution

The characteristics of the modal wavelet transform are examined by the Fourier transform for the wave shape of the basis function. The Fourier spectrum of the modal wavelet basis function is shown in Figs. 2(a)-(c), and the Fourier spectrum of typical discrete Daubechies basis functions of 4th order is shown in Fig. 2(d). The Fourier spectrum of typical discrete wavelet transform decreases the peak position and it changes to the high frequency when its level increases. On the other hand, the Fourier spectrum of the modal wavelet transform dose not decrease the peak position and it changes to a higher frequency when its level increases. In addition, the resolution between the level of modal wavelet is more than that of typical discrete wavelet. Table 1 shows the relationship of the peak frequency at each level by the Fourier transform. These levels are equivalent to each peak frequency 1/16, 2/16, 4/16, and 8/16 pixel from Table 1.

When U is a two dimensional vector velocity data, the x component is U_x, and the y component is U_y, each modal wavelet transform can be expressed by

$$S_x = WU_xW^T \quad , \quad S_y = WU_yW^T \tag{11}$$

The inverse modal wavelet transform can be given by the Eq. (12):

$$U_x = W^T S_x W \quad , \quad U_y = W^T S_y W \tag{12}$$

Because the modal wavelet transform is the orthonormal transform, the multiresolution analysis can be expressed by

$$U_x = W^T S_x W = W^T S_x^1 W + W^T S_x^2 W + \cdots + W^T S_x^{n-1} W + W^T S_x^n W \tag{13}$$

$$U_y = W^T S_y W = W^T S_y^1 W + W^T S_y^2 W + \cdots + W^T S_y^{n-1} W + W^T S_y^n W \tag{14}$$

Where $W^TS_x^1W$ and $W^TS_y^1W$ show the level 1 that is the lowest frequency, and $W^TS_x^nW$ and $W^TS_y^nW$ show the level n that is the highest frequency level. Based on the Eqs. (13) and (14), the integrated multiresolution is defined as

$$\text{Integrated Level 2} = W^TS_x^1W + W^TS_x^2W \ , \ W^TS_y^1W + W^TS_y^2W \tag{15}$$

$$\text{Integrated Level 3} = W^TS_x^1W + W^TS_x^2W + W^TS_x^3W \ , \ W^TS_y^1W + W^TS_y^2W + W^TS_y^3W \tag{16}$$

$$\vdots$$

$$\text{Integrated Level n} = W^TS_x^1W + \cdots + W^TS_x^nW, \ W^TS_y^1W + \cdots + W^TS_y^nW \tag{17}$$

The Neumann, the Diricret and the Green function types shown in Fig. 1 are used for the basis function in the modal wavelet transform. The Daubechies basis function of 4th order is used as a typical discrete wavelet transform. The integrated multiresolution were carried out by using Eq. (17) as a method of comparing these basis functions. The correlation coefficient C^L and the root mean square RMS_x^L and RMS_y^L of the x and y components are calculated by the result of the integrated multiresolution. L shows the number of integrated resolution level of the integrated multiresolution. C^L, RMS_x^L and RMS_y^L can be defend as

$$C^L = \frac{\sum_{j=1}^{n_y}\sum_{i=1}^{n_x}\left(U_{ij}^{recon^L} - \overline{U^{recon^L}}\right)\left(U_{ij}^{origin} - \overline{U^{origin}}\right)}{\sqrt{\sum_{j=1}^{n_y}\sum_{i=1}^{n_x}\left(U_{ij}^{recon^L} - \overline{U^{recon^L}}\right)^2}\sqrt{\sum_{j=1}^{n_y}\sum_{i=1}^{n_x}\left(U_{ij}^{origin} - \overline{U^{origin}}\right)^2}} \tag{18}$$

$$RMS_x^L = \frac{\sum_{j=1}^{n_y}\sum_{i=1}^{n_x}\sqrt{(U_x^{origin}{}_{ij} - U_x^{recon^L}{}_{ij})^2}}{n_x n_y} \ , \ RMS_y^L = \frac{\sum_{j=1}^{n_y}\sum_{i=1}^{n_x}\sqrt{(U_y^{origin}{}_{ij} - U_y^{recon^L}{}_{ij})^2}}{n_x n_y} \tag{19}$$

Where, U^{recon^L} shows the (i, j) value of L integrated level image decomposed by the integrated multiresolution, U^{origin} shows the (i, j) value of an original PIV image which consist of $\overline{U}$ and U'. n_x and n_y are the space resolution in x and y directions. i and j show the pixel value of the image in the x and the y directions, n_x and n_y show the numbers of pixels of the image in the x and y directions. In this study, $n_x = 16, n_y = 16$ and $L = 1$ to 16.

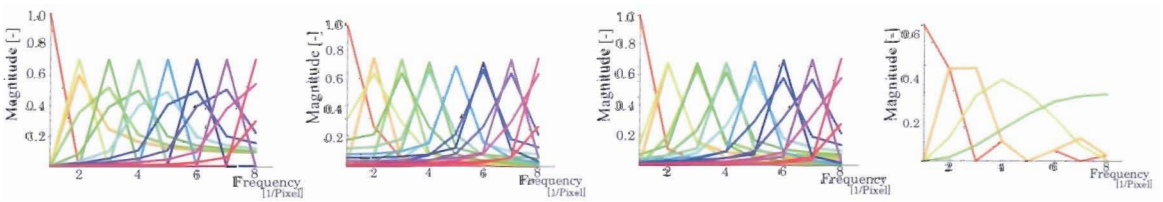

(a) Neumann (b) Dirichlet (c) Green Function (d) Daubechies 4th order

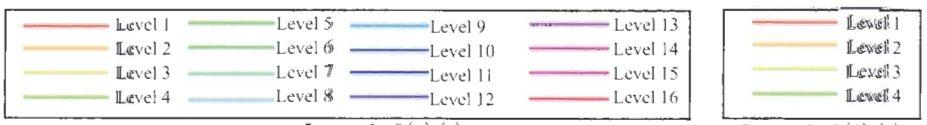

Legend of (a)-(c)

Legend of (d)-(e)

Fig. 2. Fourier spectrum of modal wavelet transform.

Table 1. Relationship between wavelet level and peak frequency.

Neumann, Dirichlet, Green Functions	Daubechies function of 4thorder	Peak frequency of Fourier transform [1/Pixel]
Level 1	Level 1	1/16
Level 2, 3	Level 2	2/16
Level 4, 5	-	3/16
Level 6, 7	Level 3	4/16
Level 8, 9	-	5/16
Level 10, 11	-	6/16
Level 12, 13	-	7/16
Level 14, 15, 16	Level 4	8/16

3. Comparison of Basis Functions by Pseudo Velocity Field

3.1 Multiresolution Analysis of Axial Flow

A pseudo velocity field of axial flow is shown in Fig. 3 based on the followin equation:

$$U = \overline{U} + U' \tag{20}$$

In the figure, velocity fluctuation U are added to uniform axial flow $\overline{U}$ in the y direction. The uniform axial flow in the direction of y is the 16 pixel × 16 pixel vector image whose x component defined as 0.0, y component as 1.0. The x and y components are the 16 × 16 vector image that is random real number in 0.0 from 0.25. The basis functions in the modal wavelet transform are compared by C^L,RMS_x^L and RMS_y^L. The multiresolution based on Neumann, Diricret, Green function types and Daubechies basis function of 4th order are shown in Figs. 4(a) - (d). These results indicate the levels 1 and 3 in the modal wavelet multiresolution and the levels 1 and 2 in the Daubechies basis function of 4th order representation. Each basis function extracts dominant flow pattern from the low frequency to the high frequency components. When it is examined in detail in the Neumann type of Fig. 4(a) and Daubechies basis function of 4th order of Fig. 4(d), the main component is extracted in the level 1 ; moreover, the small values are noticed at the level 3 in Fig. 4(a-2) and level 2 in Fig. 4(d-2). On the other hand, in the Diricret type of Fig. 4(b) and the Green function type of Fig. 4(c), it is noticed that the main component is not extracted at the level 1. In addition, at the level 3, it is evident that there exists a component that the former pseudo velocity field is not supposed to have.

Next, C^L calculated from the integrated multiresolution is shown in Fig. 5. As a result, C^L obtained from the Neumann type and the Daubechies basis function of 4th order indicates particularly the high correlation value. This indicates that the full range frequency components are accurately extracted. On the other hand, C^L obtained from the Diricret type and the Green Function types exhibit low value from the level 1 to 7. This shows that the low frequency component is not accurately extracted. And RMS_x^L and RMS_y^L calculated by the integrated multiresolution are shown in Figs. 6(a) and (b). With regard to RMS_x^L, the Neumann type and Daubechies basis function of 4th order show the low value. This result indicates that the low frequency component is accurately extracted. On the other hand, RMS_x^L in the Diricret type and the Green function type shows that the high value from the level 1 to 7. With regard to RMS_y^L the Neumann type and the Daubechies basis function of 4th order shows low value from the level 1 to 11. This result shows that the low frequency component is accurately extracted. On the other hand, RMS_y^L of the Diricret and the Green function types show the extremely high value from the level 1 to 7. This result shows that the low frequency component is not accurately extracted. As a result of analyzing pseudo axial flow, the Neumann type maybe considered as the optimum basis function because the Neumann type has similar characteristic to Daubechies basis function of 4th order, whereas the Diricret and Green function types have the lower C^L and the higher RMS^L, especially in the low level.

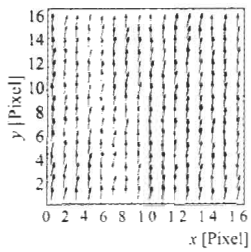

Fig. 3. Pseudo axial velocity field.

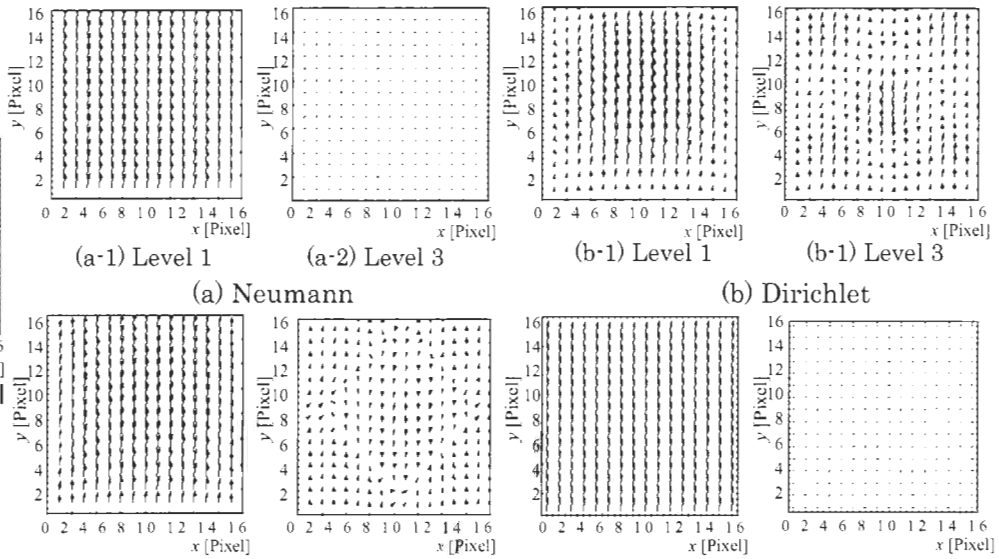

Fig. 4. Multiresolution of pseudo velocity field.

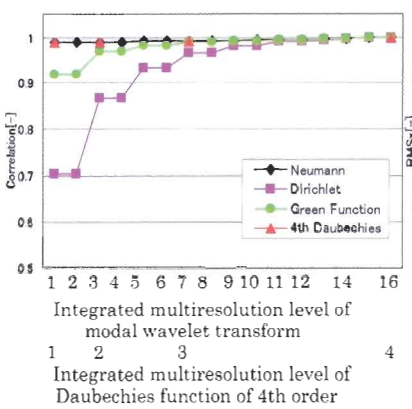

Fig. 5. Correlation of integrated multiresolution of pseudo velocity field.

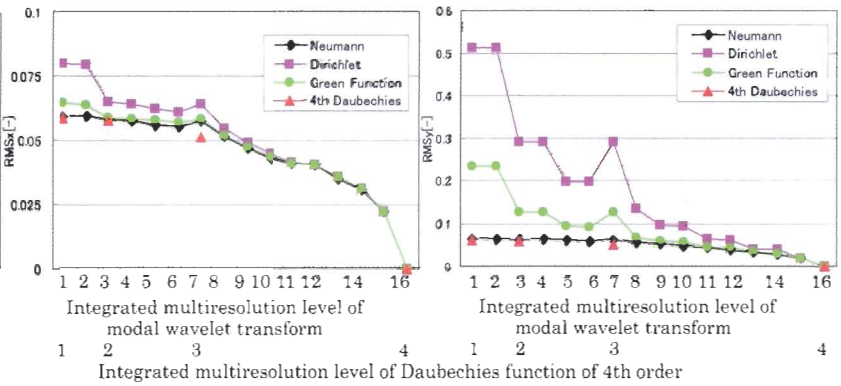

Fig. 6. RMS of integrated multiresolution of pseudo velocity field.

3.2 Multiresolution Analysis of Eddy

The pseudo velocity field of eddy is assumed as

$$U = \overline{U} + U' \quad , \quad \overline{U} = \left(\sin\frac{9\pi}{16} i + \cos\frac{9\pi}{16} j \right) \tag{21}$$

where, i and j are respectivery x and y pixel position, U' is x and y fluctuation components of the 16 pixel × 16 pixel random noise from 0.0 to 0.25. The i distribution is shown in Fig. 7. The multiresolution results calculated by Neumann type, Diricret type, Green function type and Daubechies basis function of 4th order are shown in Figs. 8(a) - (d). These figures indicate the levels 1 and 3 of the modal wavelet transform and the levels 1 and 2 of the discrete wavelet transform, respectively. The low to high frequency components are extracted by the decomposition of the pseudo eddy for all basis functions. Moreover, The component that the original velocity field dose not have is not shown in the level 1. It is understood that there exists a component that the pseudo eddy is not supposed to have.

Next, C^L calculated from the integrated multiresolution is shown in Fig. 9. C^L obtained from the Neumann type and the Daubechies basis function of 4th order indicate low correlation from the level 1 to 7. More than the integrated level 9 in each type C^L is almost same $RMS_x{}^L$ and $RMS_y{}^L$ calculated by Eq. (19) are shown in Figs. 10(a) and (b). $RMS_x{}^L$ and $RMS_y{}^L$ show the similar value irrespective of the integrated level for all basis functions.

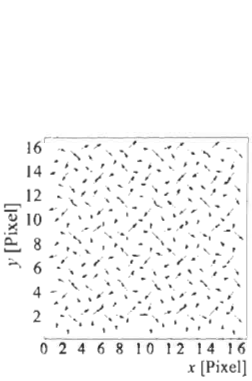

Fig. 7. Pseudo eddy velocity field.

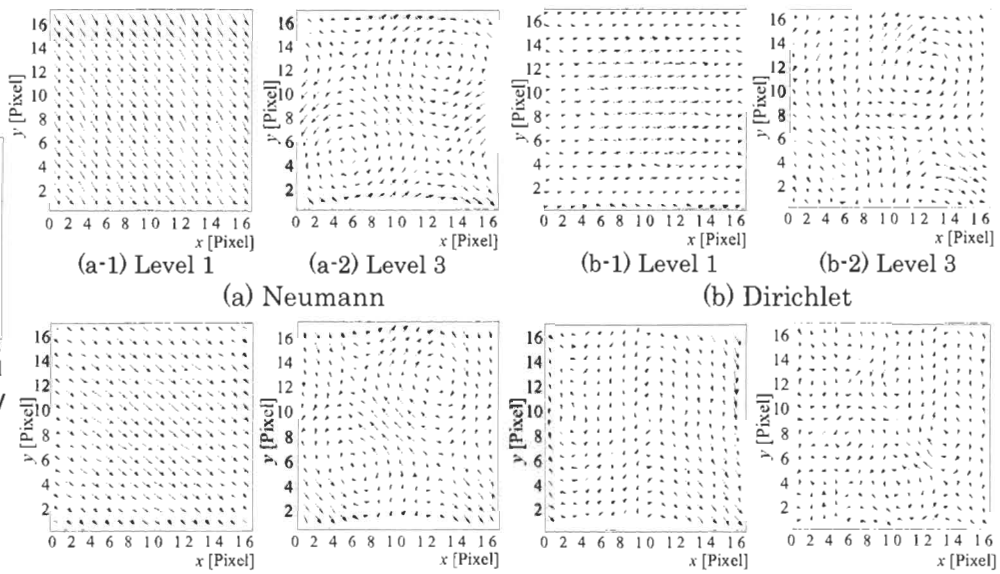

Fig. 8. Multiresolution of pseudo eddy.

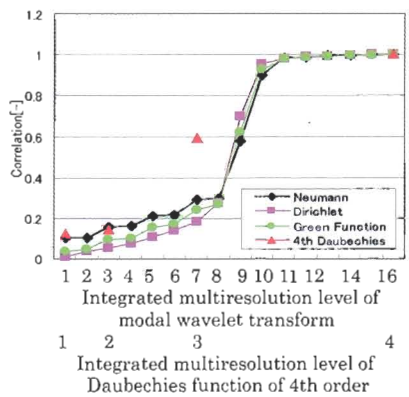

Fig. 9. Correlation of integrated multiresolution.

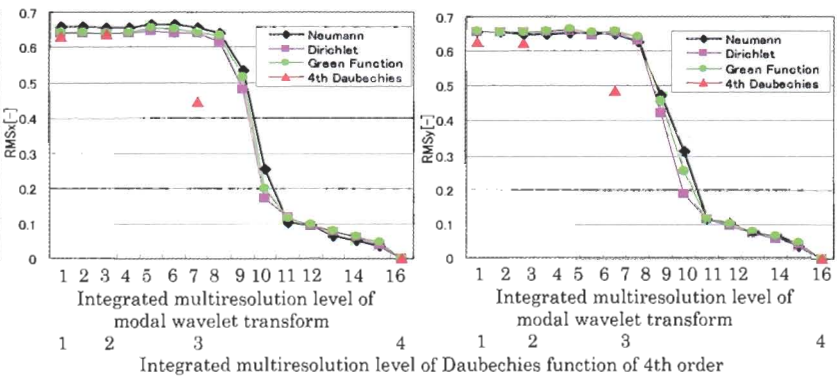

(a) Root mean square of x component (b) Root mean square of y component

Fig. 10. RMS of integrated multiresolution of pseudo eddy.

3.3 Standard PIV Velocity Field

The standard velocity field is shown in Fig. 11. It is calculated by the first and second 2D standard images that exists in the web site (http://piv. vsj. or.jp/piv/image.html) (Okamoto et al., 1997). The velocity field is the 16 pixel × 16 pixel vectors calculated by PIV correlation method. The multiresolution results calculated by the Neumann type, the Diricret type, the Green function type and Daubechies basis function of 4th order are shown in the Figs. 12(a) - (d). These figures typically show the levels 1 and 3 of the modal wavelet transform and the levels 1 and 2 of the discrete wavelet transform. On the whole, the standard velocity field can be analyzed from the low to high level, can be extracted from the low to high frequency. In each basis function, the same component are extracted for the x direction in the level 1, and in the level 3 of modal wavelet transform or the level 2 of the discrete wavelet transform. Next, C^L calculated by integrated multiresolution is shown in Fig. 13. As a result, Neumann type, Green function type and Daubechies basis function of 4th order are the high values in the integrated low level from the level 1 to 7. This shows that the low frequency elements were extracted accurately by Neumann type and Green function type. And, RMS_x^L and RMS_y^L calculated by the integrated multiresolution are shown in Figs. 14 (a) and (b). As for RMS_x^L, the Neumann, the Green function types and Daubechies basis function of 4th order exhibit the low values from the integrated level 1 to 8. This indicates that the low frequencies are extracted

accurately. On the other hand, the Diricret type exhibit the high value from the integrated level 3 to 9. This implies that the low frequency can not be extracted accurately.

According to the result of analyzing the standard velocity field, the Neumann type and the Green function type have the same characteristic as typical Daubechies function of 4th order. Because the Diricret type has the different characteristic in the low level, the optimum basis function of the modal wavelet transform is the Neumann type or the Green function type.

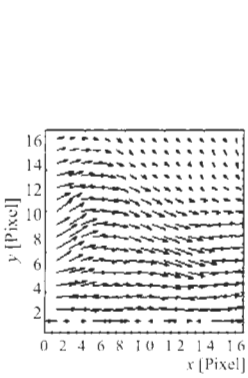

Fig. 11. Standard PIV velocity field

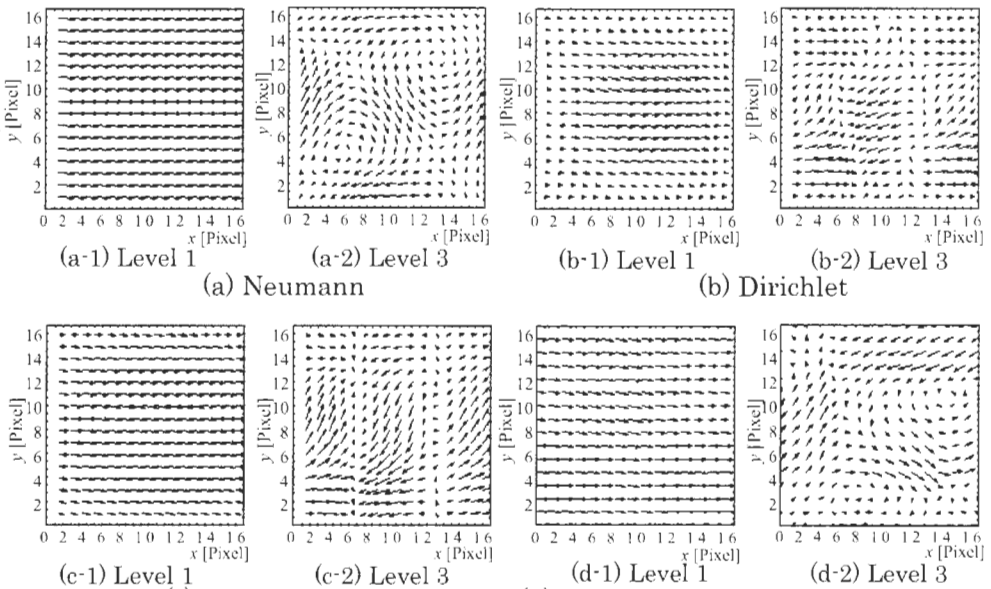

Fig. 12. Multiresolution of standard PIV velocity field.

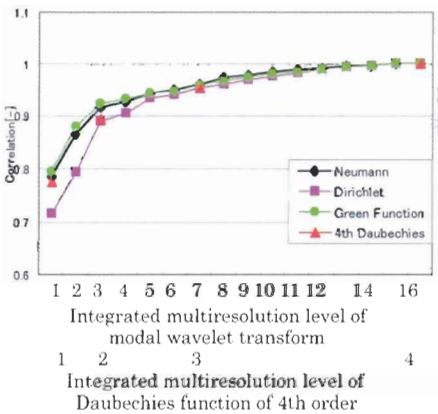

Fig. 13. Correlation of integrated multiresolution of standard PIV velocity field.

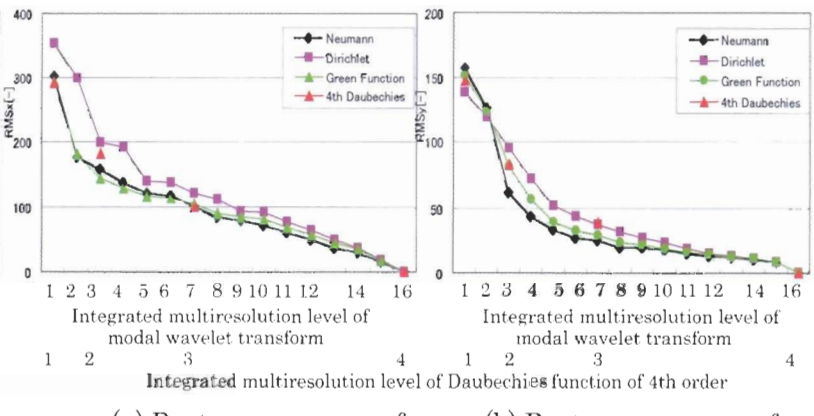

(a) Root mean square of x component (b) Root mean square of y component

Fig. 14. RMS of integrated multiresolution of standard PIV velocity field.

4. Application to Experimental PIV Vector Field

The experimental setup shown in Fig. 15 is composed of a vertical pipe, a compressor, a controller of the compressor, a laser sheet, two CMOS cameras, a pulse generator and a computer. The acrylic vertical pipe is 600 mm height, the inside diameter is 100 mm. The compressor provides the compressed air and the smoke including the tracer particles, and the flow rate can be adjusted by the controller. The light source of the laser sheet is Nd-YAG, and its output is 120 mJ. The Megaplus made by Kodak is used as the CMOS camera and its resolution is 1008 pixel × 1018 pixel. To simultaneously conduct irradiation of the laser sheet and photographing by the CMOS cameras, the

pulse generator LC880 and the application software Labview were used. And the compressed air including the smoke were supplied from the vertical pipe bottom at the flow rate of 2.43×10^{-3} m^3/sec and the mean velocity was about 0.38 m/sec and Reynolds number $Re = 2500$. The velocity field of resolution 16 pixel × 16 pixel were obtained from sequential photographs from 1 Δt sec to 180 Δt sec by correlation method. The instantaneous velocity field at 30 Δt sec is shown in Fig. 16 as a representative.

C^{μ} calculated from the integrated multiresolution is shown in Fig. 17. As a result, C^{μ} of all types indicate particular high correlation value. And RMS_x^{μ} and RMS_y^{μ} calculated by the integrated multiresolution are shown in Figs. 18(a) and (b). As for RMS_x^{μ}, the Neumann type has the smallest value. However, the values of the other types are very high irrespective of the integrated level. With regard to RMS_y^{μ}, the Neumann type has the smallest value. However, the values of the other types are very high irrespective of the integrated level. The Neumann type has similar characteristic of Daubechies basis function of 4th order; whereas, the Diricret type, the Green function type. As a result of analyzing one example of experimental PIV velocity field, the Neumann type is considered as the optimum basis function because RMS is the smallest irrespective of the integrated level.

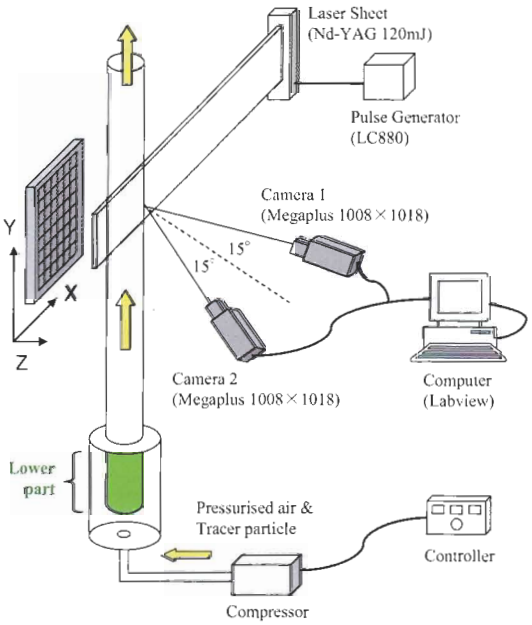

Fig. 15. Experimental setup.

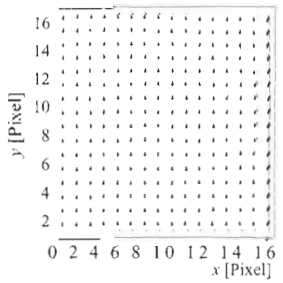

Fig. 16. Instantaneous velocity image.

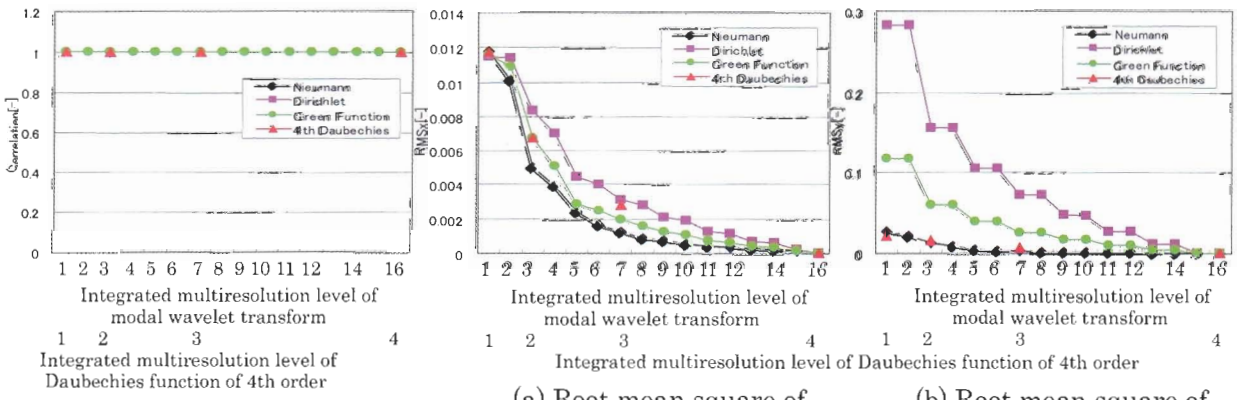

(a) Root mean square of x component

(b) Root mean square of y component

Fig. 17. Correlation of integrated multiresolution of experimental PIV vector field.

Fig. 18. RMS of integrated multiresolution of experimental PIV vector field.

5. Conclusions

The flow characteristics were extracted from the pseudo and experimental PIV velocity field by the integrated multiresolution of the modal wavelet transform and the discrete wavelet transform of the Daubechies function of 4th order. The Neumann, the Diricret and the Green function types are used for the basis function of the modal wavelet transform. The followings results can be included.

1) By analyzing a pseudo axial velocity field, the Neumann type has the highest correlation of integrated multiresolution and the lowest root mean square of integrated multiresolution. The values of the correlation and the root mean square are close to that of the typical Daubechies basis function of 4th order.

2) When analyzing a pseudo velocity field of eddy, the all basis functions have the similar values of the correlation and the root mean square of integrated multiresolution.

3) With analyzing a standard PIV velocity field, the Neumann type and Green function type have the highest value of the correlation and the lowest value of root mean square of the integrated multiresolution. The values of the correlation and the root mean square are close to that of the typical Daubechies basis function of 4th order.

4) From the result of analyzing one example of experimental PIV vector field. All types do not have large difference of the correlation. The Neumann type has the smallest value of root mean square of the integrated multiresolution. Overall, the optimum of the modal wavelet transform is the Neumann function.

Acknowledgement

This research was carried out as part of the research activity founded by the Academic frontier promotion program of MEXT in Japan.

The authors wish to thank Mr. H.Miura of Okamoto Industries Inc. for great help.

References

Camussi, R., Coherent structure identification from wavelet analysis of particle image velocimetry data, Experiments in Fluids, 32-1 (2002), 76-86.

Christensen, K. T. and Wu, Y., Visualization and Characterization of Small-Scale Spanwise Vortices in Turbulent Channel Flow, Journal of Visualization, 8-2 (2005), 177-186.

Endo, H., Marinova, I., Hayano, S., Saito, Y. and Horii, K., Modal-wavelets and their applications, Proceeding of the 2nd Japan, Australia, New Zealand Joint Seminar on Applications of Electromagnetic Phenomena in Electrical and Mechanical Systems, (2002), 24-25.

Farge, M., Wavelet transforms and their applications to turbulence, Ann Rev Fluid Mech., 24 (1992), 395-457.

Hernandes, E., Weiss, L. G., A First Course on Wavelets, (1996), CRC Press.

Kim, W., Sung, J., Yoo, J. Y. and Lee, M. H., High-definition PIV Analysis on Vortex Shedding in the Cylinder Wake, Journal of Visualization, 7-1 (2004), 17-24.

Li, H., Hu, H., Kobayashi, K., Saga, T. and Taniguchi, N., Wavelet Multiresolution Analysis of Stereoscopic Particle-Image -Velocimetry in Lobed Jet, A.I.A.A. J., 40-6 (2002), 1037-1046.

Li, H., Takei, M., Ochi, M., Saito, Y. and Horii, K., Application of Two-dimensional Orthogonal Wavelets to Multiresolution Image Analysis of a Turbulent Jet, Transactions of the Japan Society for Aeronautical and Space Sciences, 42-137 (1999), 120-127.

Okamoto, K., Nishio, S., Kobayashi, T. and Saga, T., Standard images for particle imaging velocimetry, Proc. PIV-Fukui '97, (1997), 229-236.

Özsoy, E., Rambaud, P. E., Stitou, A. and Riethmuller, L. M., Vortex characteristics in laminar cavity flow at very low mach number, Experiments in Fluids, 38-2 (2005), 133-145.

Saito, Y., Smart visualized information processing (3) -Image Processing-, The Japan Society of Applied Electromagnetics and Mechanics, 10 (2002), 170-177 (in Japanese).

Schram, C., Rambaud, P. and Riethmuller, L. M., Wavelet based eddy structure education from a backward facing step flow investigated using particle image velocimetry, Experiments in Fluids, 36-2 (2004), 233-245.

Weng, G. W., Fan, C. W., Liao, X. G. and Qin, J., Wavelet-based image denoising in (digital) particle image velocimetry, Signal Processing, 81, (2001), 1503-1512.

Author Profile

Kenji Tanaka: He received his Bachelor degree in Mechanical Engineering in 1986 from Nihon University, Tokyo Japan. He also received his M.Sc.(Eng.) degree in Mechanical Engineering in 1995 from Nihon University. He has worked for Okamoto Industries, INC. since 1986. His current position is a manager of cooperate administration. His research interests are Pneumatic conveying and PIV.

Masahiro Takei: He received his M.Sc.(Eng) in Resource Engineering in 1991 from Waseda University, Tokyo Japan. He also received his Ph.D. in Resource Engineering in 1995 from Waseda University. He has worked in Department of Mechanical Engineering, Nihon University, Tokyo Japan as an associate professor since 1995. His research interests are Computed tomography, Multiphase flow, Image processing and PIV.

Yoshifuru Saito: He received his Doctor of engineering degree in Electrical Engineering in 1975 from Hosei University. He is currently a Professor at Faculty of Engineering, Houei University. His current research interests are quantitative Computational Electromagnetics, Computational Inverse Analysis, Smart Visualized Information Processing, Power Electronics Power Magnetics, Micro Machines and Computational Literature.

Deog Hee Doh: He received B.A. at Korea Maritime University (KMU) (1985). He finished his M.Sc. degree at the graduate school of KMU(1988). He received his PhD. degree at the Department of Mechanical Engineering of the University of Tokyo, Japan in 1995. His graduate works is on the development of 3D-PTV and simultaneous measurement techniques on temperature and velocity fields for thermal flows. He worked as an invited researcher for the Advanced Fluid Engineering Research Center (AFERC) in 1995. He has been working for Korea Maritime University since 1995 at the Division of Mechanical and Information Engineering. His research interests are to develop spatial measurement techniques such as 3D-PIVs, 3D-PTVs, micro-/nano-4D-PTVs for nano-/bio- thermal flows.